

# AIRS Deconvolution and Translation from the AIRS to CrIS IR Sounders

\*\*\*\* DRAFT \*\*\*\*

Howard E. Motteler  
L. Larrabee Strow

UMBC Atmospheric Spectroscopy Lab  
Joint Center for Earth Systems Technology

March 14, 2017

## 1 Introduction

Upwelling infrared radiation as measured by the AIRS [1] and CrIS [2, 6] sounders is a significant part of the long term climate record. We would like to treat this as a single data set and often want to compare radiances, for example in the analysis of simultaneous nadir overpasses (SNOs) for sounder calibration or validation. However the instruments have different spectral resolutions, channel response functions, and band spans. As a step in addressing this problem we consider the translation of channel radiances from AIRS to standard resolution CrIS.

Translation from AIRS to CrIS involves more than simple resampling. AIRS is a grating spectrometer with a distinct response function for each channel determined by the focal plane geometry, while CrIS is a Michelson interferometer with a sinc ILS after calibration and corrections. In section 2 we show how to take advantage of our detailed knowledge of the AIRS spectral response functions (SRFs) and their overlap to deconvolve channel radiances to a resolution-enhanced intermediate representation, typically a  $0.1 \text{ cm}^{-1}$  grid, the approximate resolution of the tabulated AIRS SRFs.

The AIRS to CrIS translation then consists of two steps, deconvolution of the AIRS channel radiances to the intermediate grid, followed by reconvolution to the CrIS user grid. Section 3 gives the details and validation tests. In

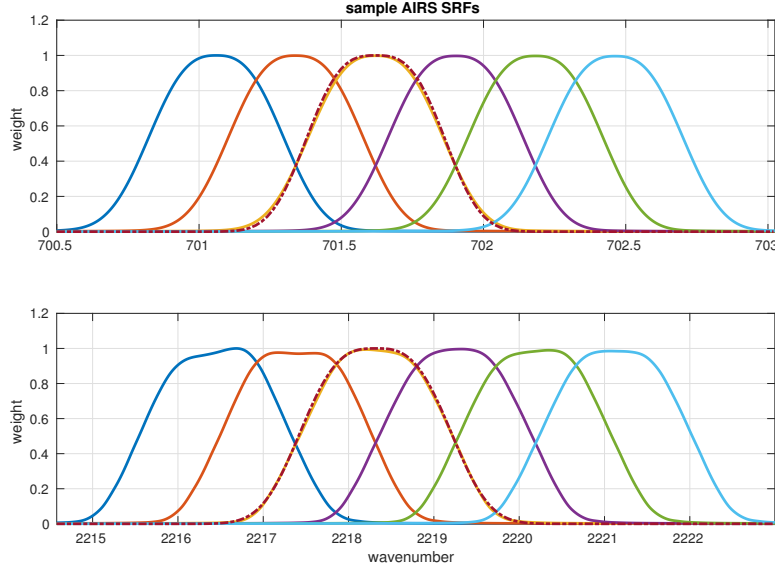


Figure 1: sample AIRS spectral response functions from the low and high ends of the band. The dashed line is a fitted symmetrical function.

section 4 we show how to further improve residuals by adding a statistically based correction. Section 5 gives some applications and conclusions.

## 2 AIRS Deconvolution

The AIRS spectral response functions model channel response as a function of frequency and associate channels with nominal center frequencies. Each AIRS channel  $i$  has an associated spectral response function or SRF  $\sigma_i(v)$  such that the channel radiance  $c_i = \int \sigma_i(v)r(v) dv$ , where  $r$  is radiance at frequency  $v$ . The center or peak of  $\sigma_i$  is the nominal channel frequency.

Figure 1 shows typical AIRS SRFs from the low and high ends of the band. Note the significant overlap in the wings. This allows the deconvolution to recover resolution beyond that of the response functions considered individually. The SRFs are not necessarily symmetrical, especially at the high end of the band. The dashed line is a 1-parameter fit of a generalized Gaussian, which we consider in more detail later in this section. Figure 2 shows channel spacing and resolving power for the AIRS L1c channel set [?]. The variable channel spacing and resolving power are due to the modular structure of the focal plane. Although not entirely regular—that is, not a

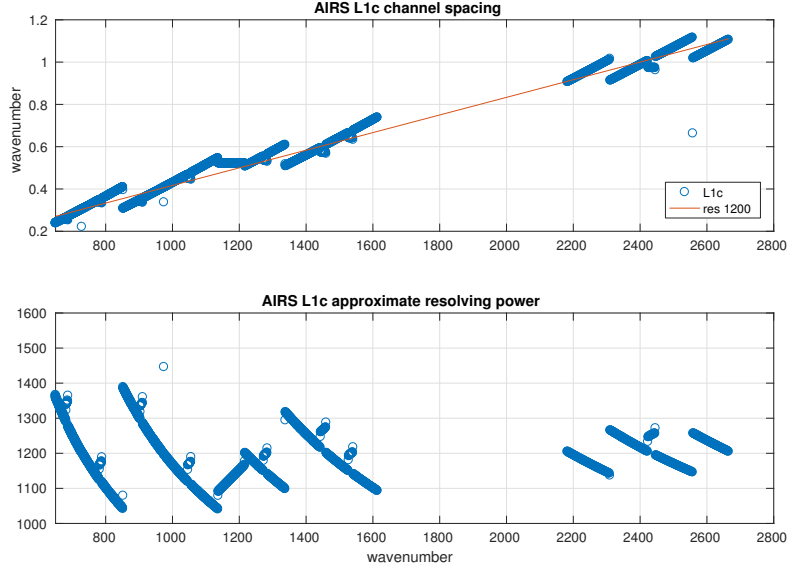


Figure 2: AIRS L1c channel spacing and derived resolving power

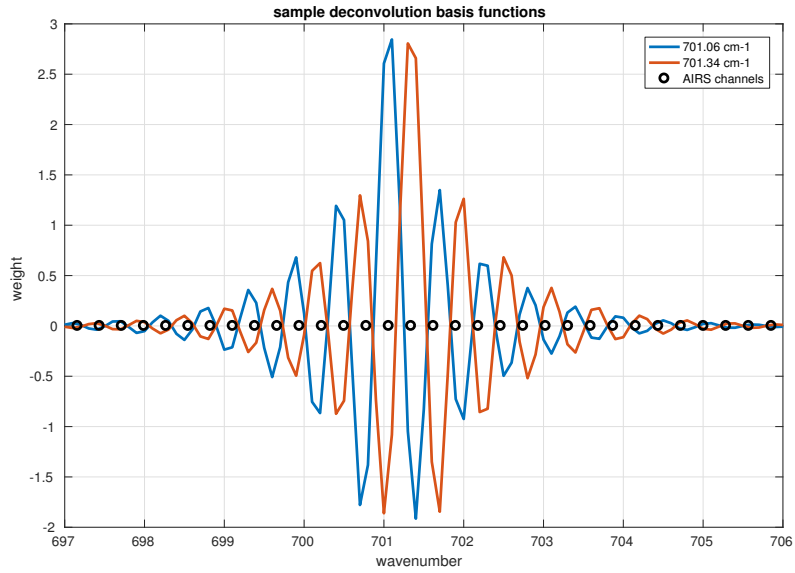


Figure 3: sample adjacent basis functions for the deconvolved AIRS radiances

simple function of frequency—the L1c channel set is more regular than the L1b channel set from which it is derived, and we mainly consider the L1c set here.

Suppose we have  $n$  channels and a frequency grid  $\vec{v}$  of  $k$  points spanning the union of the domains of the functions  $\sigma_i$ . The grid step size for our applications is often  $0.0025 \text{ cm}^{-1}$ , the kcarta resolution [4]. Let  $S_k$  be an  $n \times k$  array such that  $s_{i,j} = \sigma_i(v_j)/w_i$ , where  $w_i = \sum_j \sigma_i(v_j)$ , that is where row  $i$  is  $\sigma_i(v)$  tabulated at the grid  $\vec{v}$  and normalized so the row sum is 1. If the channel centers are in increasing order  $S_k$  is banded, and if they are not too close the rows are linearly independent.  $S_k$  is a linear transform whose domain is radiance at the grid  $\vec{v}$  and whose range is channel radiances. If  $r$  is radiance at the grid  $\vec{v}$ , then  $c = S_k r$  gives a good approximation of the channel radiances  $c_i = \int \sigma_i(v) r(v) dv$ .

In practice this is how we convolve kcarta or other simulated radiances to get AIRS channel radiances. We construct  $S_k$  either explicitly or implicitly from AIRS SRF tabulations. The matrix  $S_k$  in the former case is large but manageable with a banded or sparse representation.

Suppose we have  $S_k$  and channel radiances  $c$  and want to find  $r$ , that is, to deconvolve  $c$ . Consider the linear system  $S_k x = c$ . Since  $n < k$  for the kcarta grid mentioned above this is underdetermined, with infinitely many solutions. To solve this system we could add constraints, take a pseudo-inverse, consider a new matrix  $S_b$  with columns tabulated at some coarser grid, or some combination of the above.

For the AIRS to CrIS translation we are mainly interested in the transform  $S_b$  for SRFs at an intermediate grid, typically  $0.1 \text{ cm}^{-1}$ , the approximate resolution of the SRF measurements. Let  $\vec{v}_b = v_1, v_2, \dots, v_m$  be a  $0.1 \text{ cm}^{-1}$  grid spanning the domains of the functions  $\sigma_i$ . Similar to  $S_k$ , let  $S_b$  be an  $n \times m$  array where row  $i$  is  $\sigma_i(v)$  tabulated at the  $\vec{v}_b$  grid, with rows normalized to 1. If  $r$  is radiance at the  $\vec{v}_b$  grid, then  $c = S_b r$  is still a reasonable approximation of  $\int \sigma_i(v) r(v) dv$ .

Consider the linear system  $S_b x = c$ , similar to the case  $S_k x = c$  above, where we are given  $S_b$  and channel signals  $c$  and want to find radiances  $x$ . Since  $n < m < k$ , as with  $S_k$  the system will be underdetermined, but more manageable because  $m$  is approximately 40 times less than  $k$ . After some preliminary tests we settled on a Moore-Penrose pseudoinverse for  $S_b^{-1}$ . Then  $x = S_b^{-1} c$  gives us deconvolved radiances at the SRF tabulation grid. Figure 3 shows adjacent typical basis function for the deconvolution, that is, columns of the pseudo-inverse  $S_b^{-1}$ . The functions are vaguely sinc-like, though the negative excursions are significantly greater. For each channel  $c$ , the columns show the span of influence of  $c$  in the deconvolution.

The AIRS deconvolution gives a significant resolution enhancement, though at the cost of added artifacts and noise. Figure 4 shows spectra for a simulated deconvolution together with the direct convolution of kcarta  $0.0025\text{ cm}^{-1}$  radiances to the  $0.1\text{ cm}^{-1}$  intermediate grid, for fitting profile 1. The deconvolution is done by convolving kcarta radiances to the AIRS L1c channel set to get “true AIRS” and then deconvolving this to the  $0.1\text{ cm}^{-1}$  grid, as discussed above.

The direct convolution is for a hypothetical grating spectrometer with a resolving power of 2000, oversampled to the  $0.1\text{ cm}^{-1}$  grid. The choice of basis functions for reference truth for the intermediate  $0.1\text{ cm}^{-1}$  grid is not obvious, since the deconvolution is undoing—at least to some extent—the effects of the AIRS SRF convolutions. The response function we used for this, and for the “L1d basis” discussed below, is a generalized Gaussian of the form

$$w = \exp\left(-\left(\frac{(x - v_0)^2}{2c^2}\right)^{1.5}\right)$$

where  $c = \text{FWHM}/2.355$  and  $v_0$  is the desired channel center. The exponent 1.5 is chosen to give an approximate match to AIRS SRFs with the same FWHM, though without the fine structure and variation of the latter.

Figure 1 shows two such functions paired with AIRS SRFs with the same FWHM. Figure 5 shows the mean and standard deviation of the difference of the deconvolved minus the directly convolved radiances for the 49 fitting profiles [3, 5], after translation to brightness temperatures. The residuals are large and mainly significant for understanding limitations of the deconvolution. The residuals can be reduced dramatically by convolving the  $0.1\text{ cm}^{-1}$  intermediate grid to the channel grid for an idealized grating instrument with reduced resolving power. Define an L1d basis with generalized gaussian SRFs,  $\text{FWHM} = v/\text{resolving power}$ , and  $dv = \text{FWHM}/2$  with the  $dv$ -spaced channel steps starting at  $v_0$ . Note this is not over-sampled, in contrast with the regular spacing used for the  $0.1\text{ cm}^{-1}$  intermediate grid.

Figure 6 shows residuals for reconvolution to such an L1d basis with resolving power of 1200, the nominal AIRS resolution. For this comparison both the reference truth (true L1d) and the reconvolution (L1c to L1d) are done to L1d channel sets with the same resolving power and starting channel. An L1d set with a resolving power of 1200 gives a significant improvement over the residual for an unreconvolved resolving power of 2000. Figure 7 shows residuals for a resolving power of 700. This is less than the the residual for unapodized CrIS shown in section 3 that we use as the starting point for our AIRS to CrIS translations.

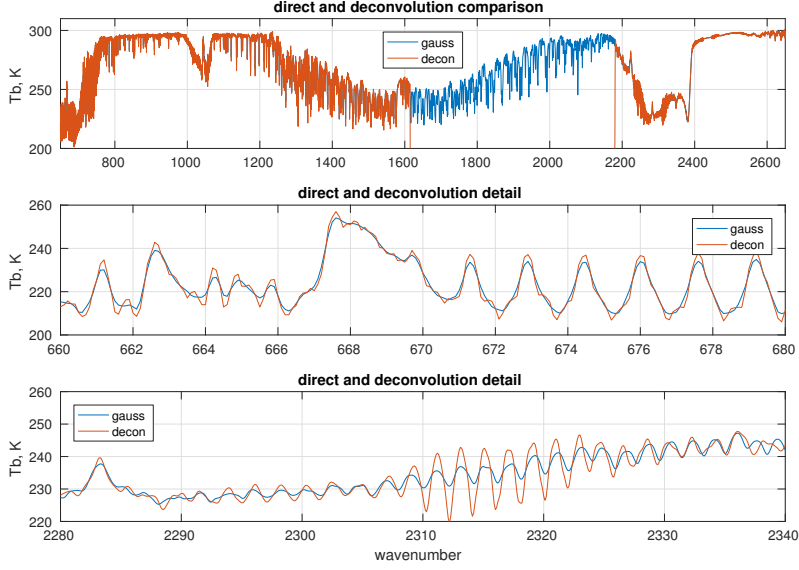


Figure 4: spectra from fitting profile 1 for the L1c deconvolution and direct convolution to the  $0.1 \text{ cm}^{-1}$  intermediate grid with an oversampled resolving power of 2000

This is only half the best AIRS resolving power of 1400 in the LW. Resolution is lost in shifting channel centers. The L1d residuals for a resolving power of 700 and 1200 depend in part on the starting channel, and so on how the SRF peaks line up and match with the L1c set. The residuals above are the result of a rough fit for  $v_0$ . For a resolving power of 1200 this is the first L1c channel, while for 700 it was the first channel plus  $0.2 \text{ cm}^{-1}$ .

Despite the resolution loss, deconvolution is significantly better than interpolation for the L1c to L1d translation. We consider two cases. For the first, start with true L1c and interpolate radiances directly to the L1d grid with a cubic spline. For the second, interpolate true L1c to the  $0.1 \text{ cm}^{-1}$  intermediate grid with a cubic spline and convolve this to the L1d channel set. Figure 8 shows interpolated L1d minus true L1d. The two-step interpolation works a little better than the simple spline, but is still much larger than the residual for translation with deconvolution.

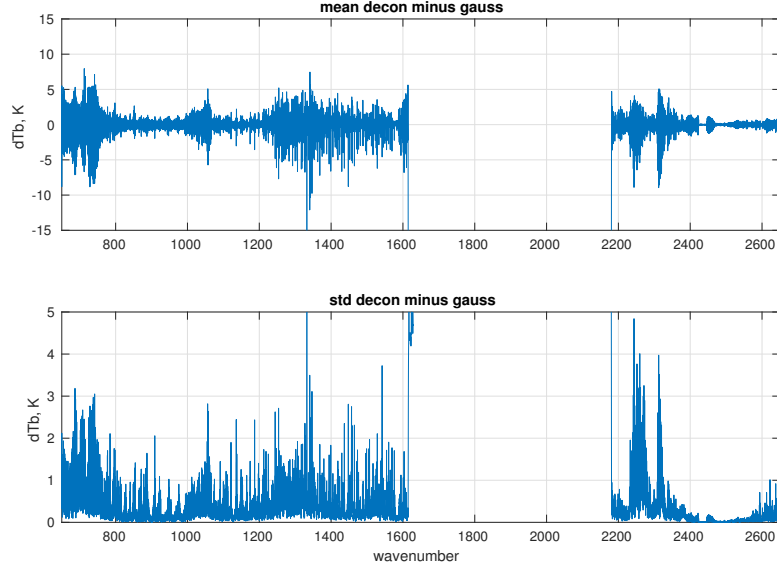


Figure 5: mean and standard deviation over the 49 fitting profiles for the L1c deconvolution minus direct convolution to the  $0.1 \text{ cm}^{-1}$  intermediate grid with an oversampled resolving power of 2000

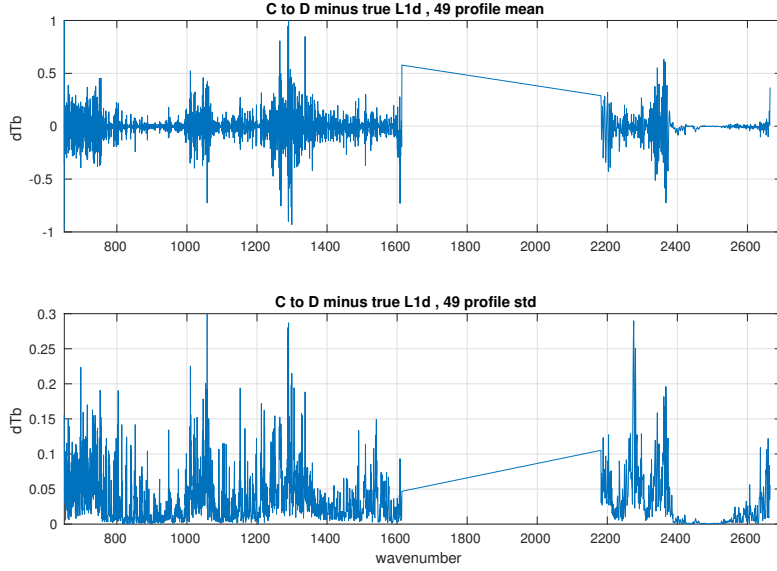


Figure 6: mean and standard deviation over the 49 fitting profiles for the L1c deconvolution minus reconversion to an L1d basis with  $v_0 = 649.622 \text{ cm}^{-1}$  and a resolving power of 1200

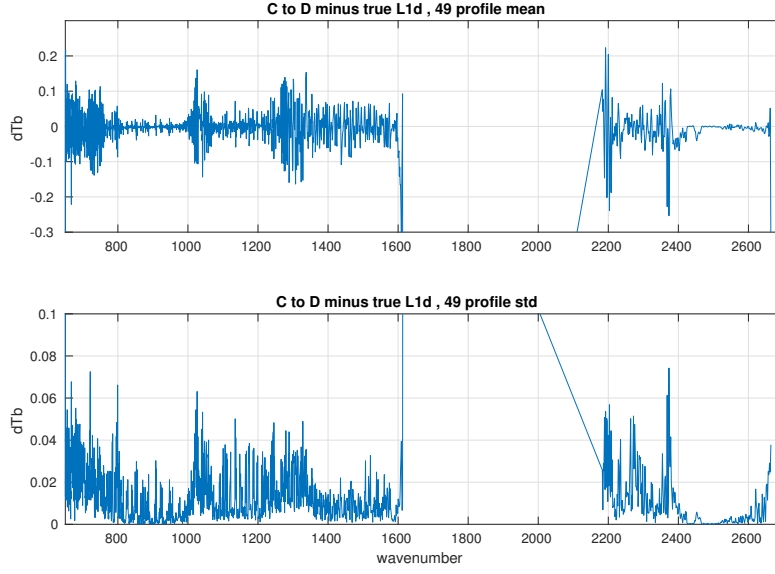


Figure 7: mean and standard deviation over the 49 fitting profiles for the L1c deconvolution minus reconvolution to an L1d basis with  $\nu_0 = 649.822 \text{ cm}^{-1}$  and a resolving power of 700

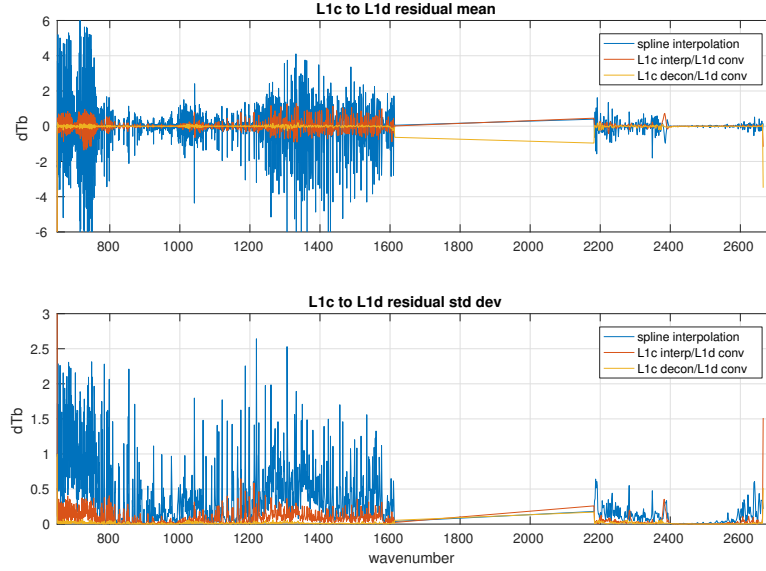


Figure 8: spline interpolation, interpolation with convolution, and deconvolution with convolution for the AIRS L1c to L1d translation with  $\nu_0 = 649.822 \text{ cm}^{-1}$  and a resolving power of 700



### 3 AIRS to CrIS translation

For the CrIS standard resolution mode the channel spacing is  $0.625\text{ cm}^{-1}$  for the LW,  $1.25\text{ cm}^{-1}$  for the MW, and  $2.5\text{ cm}^{-1}$  for the SW bands. The first step in the AIRS L1c to CrIS translation is to deconvolve the AIRS channel radiances to the  $0.1\text{ cm}^{-1}$  intermediate grid, the nominal AIRS SRF resolution. Then for each CrIS band, we

- find the AIRS and CrIS band intersection
- apply a bandpass filter to the deconvolved AIRS radiances to restrict them to the intersection, with a rolloff outside the intersection
- reconvolve the filtered spectra to the CrIS user grid

Translations are validated by comparison with calculated reference truth. For the results presented in this section we start with 49 fitting profiles spanning a significant range of atmospheric conditions [3, 5]. Upwelling radiance is calculated at a  $0.0025\text{ cm}^{-1}$  grid with kcarta [4] over a band spanning the AIRS and CrIS response functions. “True AIRS” is calculated by convolving the kcarta radiances with AIRS SRFs, and “true CrIS” by convolving kcarta radiances to a sinc basis at the CrIS user-grid specifications. AIRS is then translated to CrIS to get “AIRS CrIS”, and this is compared with true CrIS. This validation assumes perfect knowledge of the AIRS and CrIS instrument response functions and so gives only a lower bound on residuals, and on how well the translations can work in practice. The better we know the response functions, the closer real translations can approach these limits.

Figures 9, 10, and 11 show the mean and standard deviation of true CrIS minus AIRS CrIS for the 49 fitting profiles, with and without Hamming apodization, for each of the CrIS bands. Figures 12 and 13 summarize the mean and standard deviation of the residuals for Hamming apodized radiances. The residual has a high frequency component with a period of 2 channel steps that is significantly reduced by the apodization. The constant or DC bias (the mean of the residuals over frequency) is very close to zero for the apodized residuals:  $0.002\text{ K}$  for the LW,  $-0.005\text{ K}$  for the MW, and  $0.001\text{ K}$  for the SW.

Deconvolution is significantly better than interpolation for the AIRS to CrIS translation. We consider two cases. For the first, start with true AIRS and interpolate radiances directly to the CrIS user grid with a cubic spline. For the second, interpolate true AIRS to the  $0.1\text{ cm}^{-1}$  intermediate grid

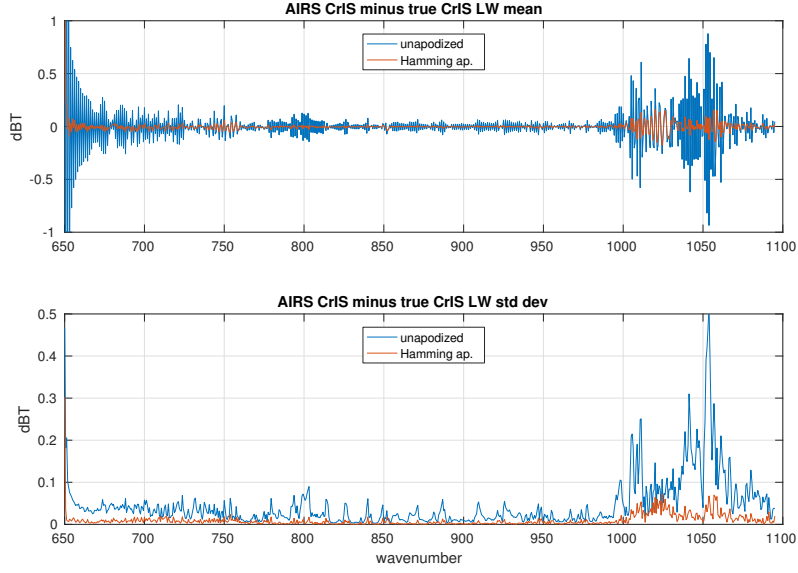


Figure 9: Mean and standard deviation of unapodized and Hamming apodized AIRS CrIS minus true CrIS, for the CrIS LW band

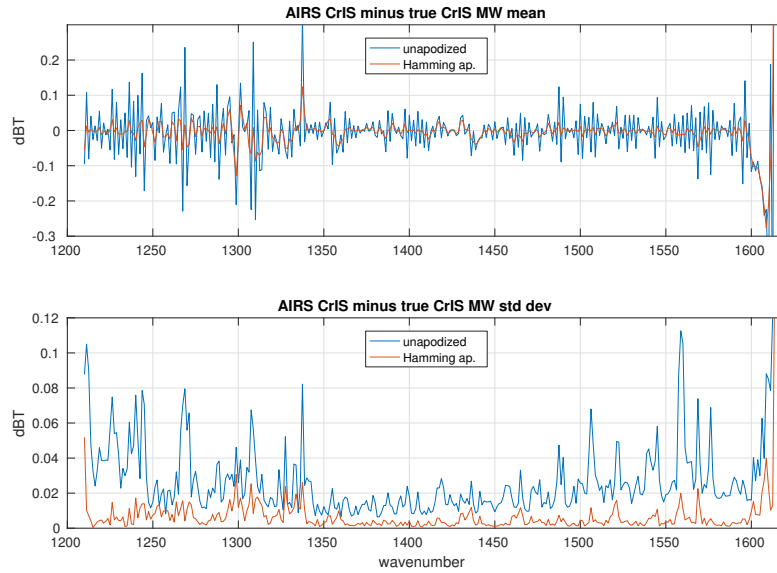


Figure 10: Mean and standard deviation of unapodized and Hamming apodized AIRS CrIS minus true CrIS, for the CrIS MW band

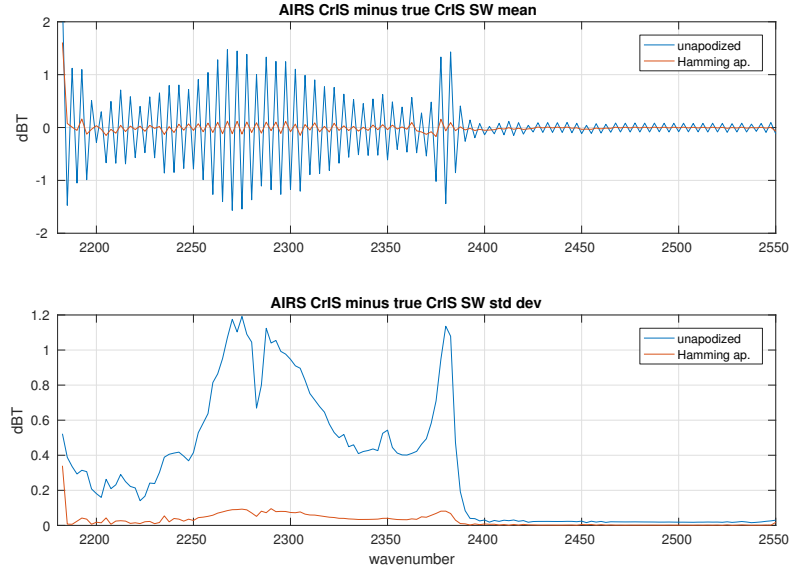


Figure 11: Mean and standard deviation of unapodized and Hamming apodized AIRS CrIS minus true CrIS, for the CrIS SW band

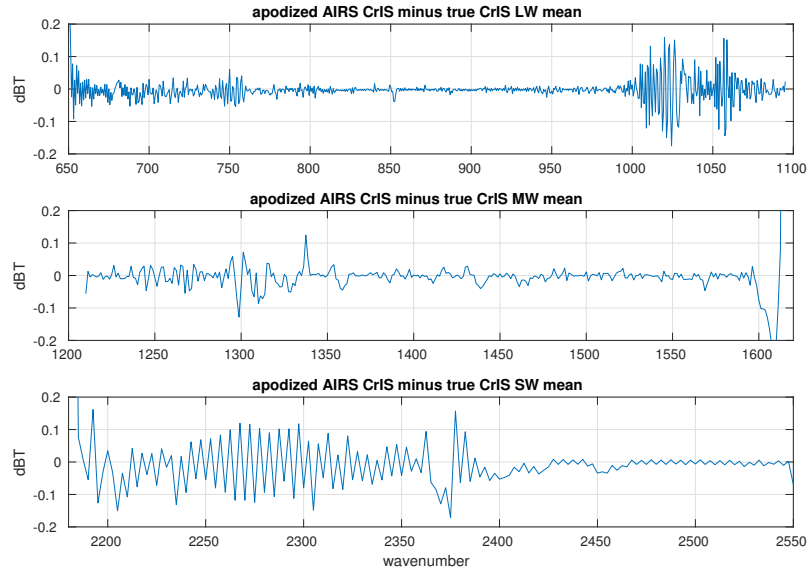


Figure 12: Mean of apodized residuals for all three CrIS bands

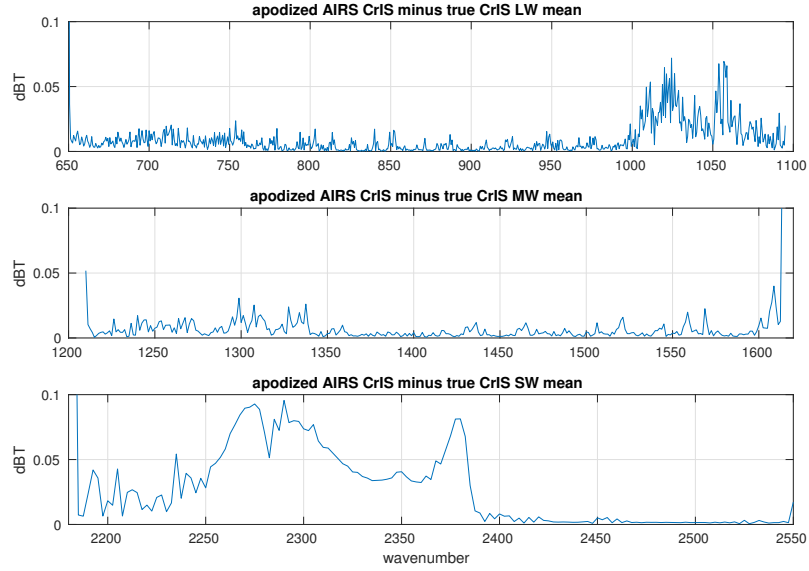


Figure 13: Standard deviation of apodized residuals for all three CrIS bands

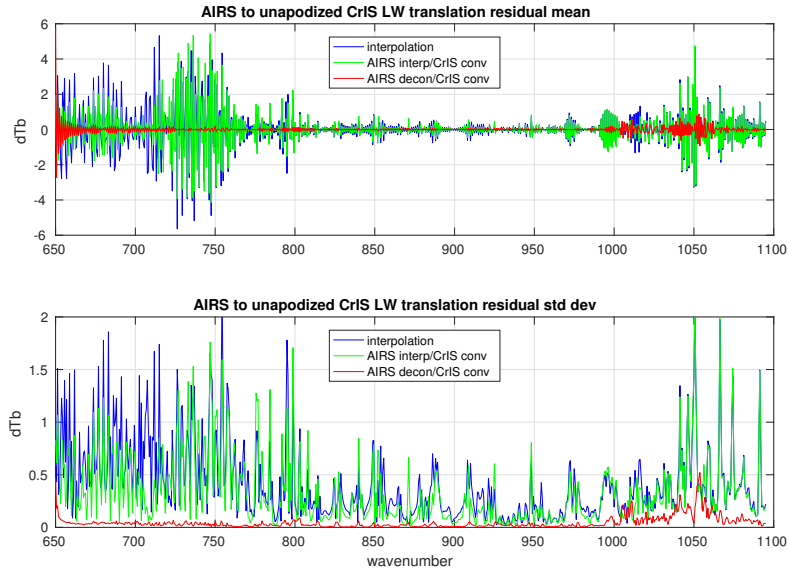


Figure 14: spline interpolation, interpolation with convolution, and deconvolution with convolution for the CrIS LW band

with a cubic spline and then convolve this to the use CrIS user grid. Figure 14 shows interpolated CrIS minus true CrIS for the LW band, without apodization. The two-step interpolation works a little better than the simple spline, but both residuals are significantly larger than for the translation with deconvolution. Results for the MW are similar, while the unapodized comparison is less clear for the SW. With Hamming apodization, the residuals with deconvolution are significantly less than interpolation for all three bands.

## 4 Statistitcal Refinement

Residuals for the AIRS to apodized CrIS translation are already small, and have no significant DC bias. But there is some regularity in the residual, including an oscillation with period two channel steps. We show that a linear correction can significantly reduce this residual. This is a standard technique but worth describing briefly because the reduction is significant.

For these tests we start with kcarta radiances calculated from a set of 7377 radiances calculated from mostly cloudy AIRS profiles, spanning several consecutive days. These are split randomly into dependent and independent sets. Bias or regression coefficients are taken from the dependent set, and tests are done on the independent set. As with the 49 profile set “true AIRS” channel radiances are calculated by convolving with AIRS SRFs and “true CrIS” by convolving to the CrIS instrument specifications.

Note the difference in statistical approaches here and in section 3. There we used a small, largely uncorrelated set of 49 profiles chosen to span all common clear atmospheric conditions, and intended for developing and testing radiative transfer codes. For the statistical correction we use a more typical mix of clear and cloudy data spanning several days, moderately correlated, and large enough to allow for partition into significant dependent and independent sets.

Figure 15 is a comparison of bias, linear, and quadratic corrections for a representative dependend/independent partition. The residuals vary with the partition but the standard deviation is consistently significantly less for the linear and quadratic cases. The linear and quadratic corrections are nearly identical, the quadratic coefficient is very close to zero. Figure 16 shows the weights for the linear fits shown above. The  $a$  weight is very close to 1 and the  $b$  weight to earlier bias values.

Figures 17 and 18 show the linear correction is giving a similar significant improvement in the MW standard deviation in comparison with the LW,

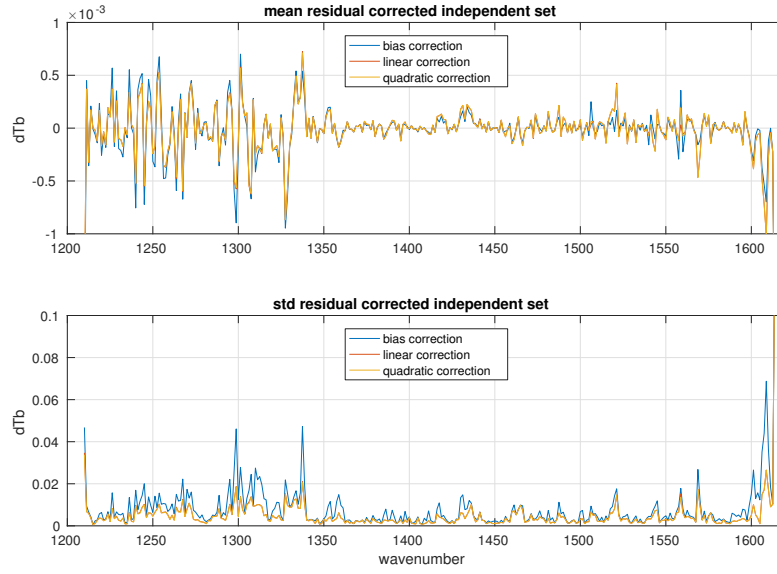


Figure 15: Mean and standard deviation of LW corrected apodized residuals for the independent subset of the 7377 profile set

and a small improvement in the SW. As in the LW the mean residuals vary significantly depending on the dependent/independent partition, but the standard deviations are relatively stable.

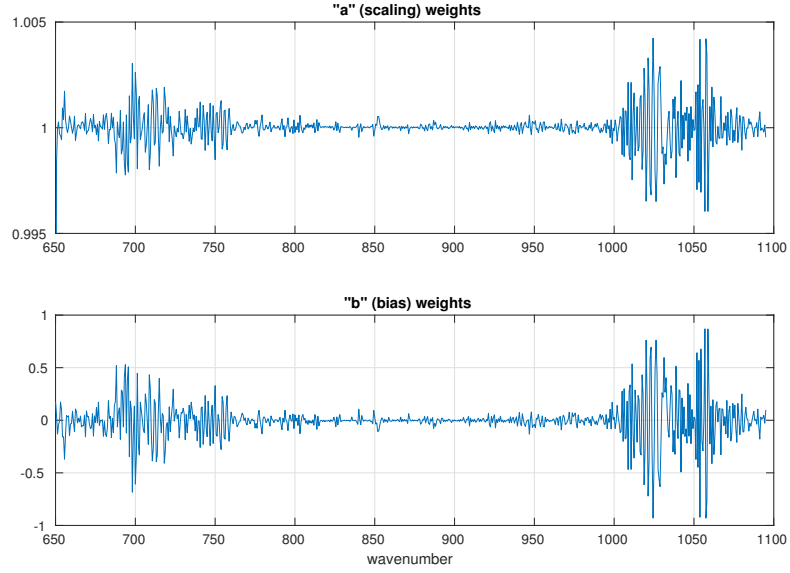


Figure 16: LW  $a$  and  $b$  weights for the linear correction  $ax + b$

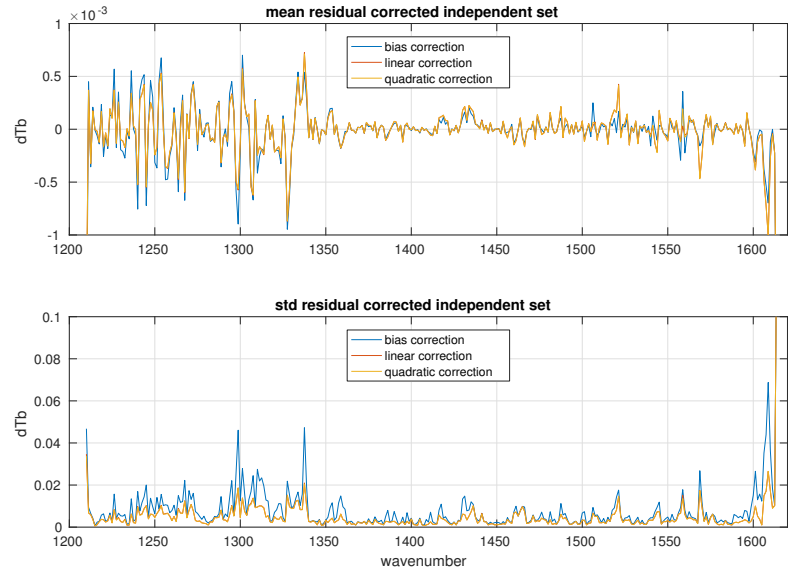


Figure 17: Mean and standard deviation of MW corrected apodized residuals for the independent subset of the 7377 profile set

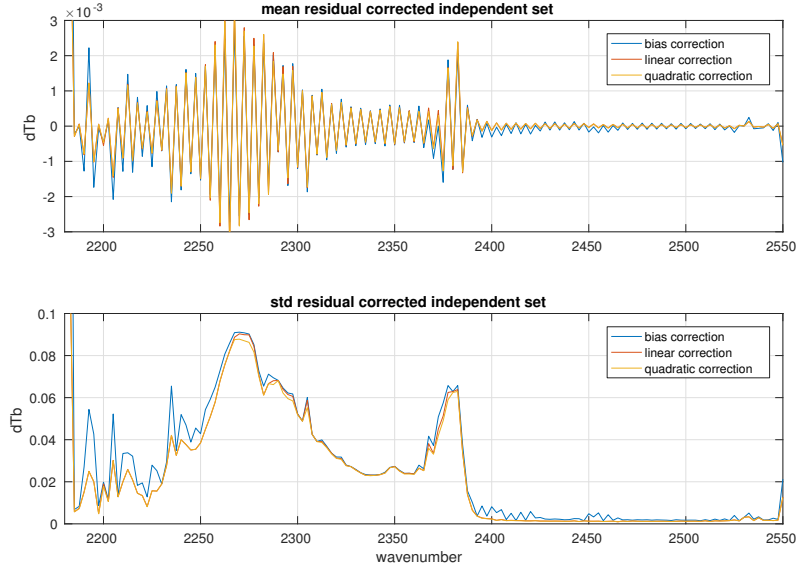


Figure 18: Mean and standard deviation of SW corrected apodized residuals for the independent subset of the 7377 profile set

## 5 Applications and conclusions

### References

- [1] H. H. Aumann, M. T. Chahine, C. Gautier, M. D. Goldberg, E. Kalnay, L. M. McMillin, H. Revercomb, P. W. Rosenkranz, W. L. Smith, D. H. Staelin, L. L. Strow, and J. Susskind. AIRS/AMSU/HSB on the aqua mission: design, science objectives, data products, and processing systems. *IEEE Transactions on Geoscience and Remote Sensing*, 41:253–264, Feb. 2003.
- [2] Y. Han, H. Revercomb, M. Crompt, D. Gu, D. Johnson, D. Mooney, D. Scott, L. Strow, G. Bingham, L. Borg, Y. Chen, D. DeSlover, M. Esplin, D. Hagan, X. Jin, R. Knuteson, H. Motteler, J. Predina, L. Suwinski, J. Taylor, D. Tobin, D. Tremblay, C. Wang, L. Wang, L. Wang, and V. Zavyalov. Suomi NPP CrIS measurements, sensor data record algorithm, calibration and validation activities, and record data quality. *Journal of Geophysical Research (Atmospheres)*, 118:12734, Nov. 2013.
- [3] L. Strow, S. Hannon, S. De Souza-Machado, H. Motteler, and D. Tobin.



An overview of the airs radiative transfer model. *Geoscience and Remote Sensing, IEEE Transactions on*, 41(2):303–313, Feb 2003.

- [4] L. Strow, H. E. Motteler, R. G. Benson, S. E. Hannon, and S. D. Souza-Machado. Fast computation of monochromatic infrared atmospheric transmittances using compressed look-up tables. *Journal of Quantitative Spectroscopy and Radiative Transfer*, 59(35):481 – 493, 1998. Atmospheric Spectroscopy Applications 96.
- [5] L. L. Strow, S. E. Hannon, S. De-Souza Machado, H. E. Motteler, and D. C. Tobin. Validation of the atmospheric infrared sounder radiative transfer algorithm. *Journal of Geophysical Research: Atmospheres*, 111(D9), 2006. D09S06.
- [6] L. L. Strow, H. Motteler, D. Tobin, H. Revercomb, S. Hannon, H. Buijs, J. Predina, L. Suwinski, and R. Glumb. Spectral calibration and validation of the Cross-track Infrared Sounder on the Suomi NPP satellite. *Journal of Geophysical Research (Atmospheres)*, 118:12486, Nov. 2013.